Near Surface Geophysics

Near Surface Geophysics, 2022, **20**, 135–146 doi: 10.1002/nsg.12196

Check for updates

Choosing optimal model parameterization for improving the accuracy of refraction seismic tomography

Gleb Stanislavovich Chernyshov[1,2], Anton Albertovich Duchkov[1,2] and Ivan Yurievich Koulakov[1,2]

[1]*Trofimuk Institute of Petroleum Geology and Geophysics SB RAS, Pr. Koptyuga 3, Novosibirsk, 630090, Russia, and* [2]*Novosibirsk State University, St. Pirogova 1, Novosibirsk, 630090, Russia*

Received November 2020, revision accepted January 2022

ABSTRACT

Seismic ray tomography is a popular tool for reconstructing seismic velocity models from traveltime data. Here we study how the model parameterization affects the resolution and accuracy of the tomographic inversion for the near-surface model building. In particular, we consider the weighting of the elements of the model perturbation vector based on the values of the initial velocity model. When the model parameters are defined in terms of velocities, then the tomographic-inversion resolution is better for the shallow part but degrades for the deeper part of the model. The opposite is true when the model parameters are defined in terms of slowness values. This effect is associated with the method of forming the tomographic matrix. When linearizing the tomography problem for different model parameters, the matrix elements have different weight coefficients. This affects the inversion results and can lead to large errors. We suggest a new parameterization (in-between the velocity and the slowness) that provides better quality of the tomographic inversion and balanced resolution between the shallow and deeper part of the model. The good performance of this new parameterization is confirmed by a series of synthetic tests and one real-data example.

Key words: data processing, near-surface, seismic, Tomography.

INTRODUCTION

Seismic refraction methods are widely used for constructing geological models at various scales: the Earth's crust in regional studies (Suvorov *et al*., 2002), shallow hydrogeological and waste disposal problems (Lanz *et al*., 1998), mapping archaeological sites (Arciniega-Ceballos *et al*., 2009; Di Fiore *et al*., 2016), etc. Further development of geophysical methods in the near-surface characterization includes the multichannel analysis of surface waves (Park, 1999), combining refraction and reflection seismic processing (Maries *et al*., 2016; Sun *et al*., 2020) and combining seismic and electrical surveys (Cercato and De Donno, 2018).

The main refraction-seismic processing methods include the plus-minus method (Hagedoorn, 1959), the generalized reciprocal method (Palmer, 2015) and seismic tomography (Nolet, 1987, 2012). The linearized tomographic inversion was first introduced in global seismology to study the mantle structure. But now it is widely used in exploration and near-surface seismology (Schicht *et al*., 2007; Yilmaz, 2015). The problem of tomographic inversion is non-unique, and various regularization methods are used to obtain a solution (Zelt, 2011). It is non-trivial to choose a proper regularization method and ensure a geologically meaningful model (c.f., Palmer, 2015). In particular, various model parameterizations are used: layered model (Zelt and Smith, 1992); discrete tomography (Varga *et al*., 2015); wavelet basis functions (Tikhotskii *et al*., 2011); and multiple-grid parameterization (Tong *et al*., 2019). Trabi (2018) discusses how differences in the model

E-mail: chernyshovgs@ipgg.sbras.ru

© 2022 European Association of Geoscientists & Engineers

Table 1 Mean absolute error (m/s) of the velocity reconstruction in different regions

Model parameterization	Shallow part (m/s)	All depths (m/s)
Velocity	20.7	84.3
Slowness	21.7	79.9
New	20.9	79.6
Alternating with velocity and slowness	21.0	81.8

parameterization (velocity perturbations vs. slowness perturbations) affect the results of the tomographic inversion. Zelt (2011) also mentions that normalization by the reference model values results in penalizing relative quantities as opposed to absolute values. Here we revisit the problem of weighing the elements of the model vector (unknown model perturbations) in order to improve the resolution and accuracy of the tomographic inversion for near-surface model building. In this paper, we consider the influence of the model-parameterization choice on tomographic inversion results. We also propose an alternative model parameterization that is advantageous for recovering shallow and deep anomalies of seismic velocities.

The rest of the paper is organized as follows. First, we briefly discuss the theoretical basics of seismic ray tomography focusing on various model parameterizations. Then we perform a series of synthetic tests and a real-data example comparing different parameterizations and advantages of the proposed new one. We conclude with a summary of the results.

METHOD

Let us briefly review the standard formulation of the ray tomographic problem (Zelt, 2011). The tomography problem is based on the traveltime of the wave along the ray path:

$$t(c,r) = \int_{P_{cr}} \frac{\mathrm{d}s}{m(x,z)}, \tag{1}$$

where $t(c, r)$ is traveltime between source c and receiver r, P is a ray trajectory, and $\mathbf{m}(x, z)$ is the velocity at (x, z) coordinates.

The linearization process expresses the dependence of the unknown anomalies of the initial velocity model and the time misfits along the seismic rays. We start with an initial velocity model, then look for small unknown perturbations solving the tomographic linear system:

$$t(c,r) = \int_{P_{cr}} \frac{\mathrm{d}s}{m_0 + \delta m} \approx \int_{P_{cr}} \frac{\mathrm{d}s}{m_0} - \int_{P_{cr}} \frac{\delta m}{m_0^2}\mathrm{d}s = t_0(c,r) - \int_{P_{cr}} \frac{\delta m}{m_0^2}\mathrm{d}s, \tag{2}$$

$$\delta t(c,r) = t_0(c,r) - t(c,r) = \int_{P^0_{cr}} \frac{\delta m}{m_0^2}\mathrm{d}s = A\langle \delta m(x,z)\rangle, \tag{3}$$

$$A\,\delta m = \delta t, \tag{4}$$

where $\delta m = m - m_0$ is a model perturbation, m is the velocity in the true model, m_0 is the velocity in the reference model; $\delta t = t - t_0$ is traveltime misfit, t is observed traveltimes, t_0 is computed traveltime from the reference model m_0; **A** is the tomographic matrix (each element corresponds to the traveltime misfit for a particular ray caused by the model perturbation in a particular grid cell).

Note that we can rewrite this tomographic linear system (equation (4)) in various forms by applying a scaling of the model-parameter space, which is a particular form of the right-preconditioning (Luo *et al.*, 2015):

$$(A\,W)\,\delta\,\tilde{m} = \delta t,, \tag{5}$$

where **W** is the diagonal scaling matrix with elements w_{ii} and $\delta\,\tilde{m} = W^{-1}\,\delta m$ is a new set of model parameters after scaling.

This diagonal scaling matrix **W** is a changing model parameterization, including two parameterizations that naturally appear in the literature (Zelt, 2011):

- slowness model parameterization, where $w_{ii} = 1$ (model parameters δm have physical units of s/m);
- velocity model parameterization, where $w_{ii} = 1/v_{0i}^2$ (model parameters $\delta m\prime$ have physical units of m/s).

These two model parameterizations are related to each other as follows: $\delta m\prime_i = v_{0i}^2\,\delta m_i$. Given that the reference model v_0 is normally increasing with depth, one can see that the velocity perturbations $\delta m\prime_i$ of the same order at greater depth correspond to smaller smoothness perturbations δm_i (by a factor of v_{0i}^2). This is equivalent to saying that the linear system (equation (5)) in the velocity parameterization is less sensitive to deep anomalies in the model parameters. Also, note that equation (5) allows for a family of diagonal scaling matrices W_σ based on using the reference model v_0, where the elements have the form:

$$w_{\sigma ii} = 1/v_{0i}^{\sigma}. \tag{6}$$

18730604, 2022, 2, Downloaded from https://onlinelibrary.wiley.com/doi/10.1002/nsg.12196 by Trofimuk Institute of Petroleum Geology and Geophysics SB RAS, Wiley Online Library on [28/11/2024]. See the Terms and Conditions (https://onlinelibrary.wiley.com/terms-and-conditions) on Wiley Online Library for rules of use; OA articles are governed by the applicable Creative Commons License

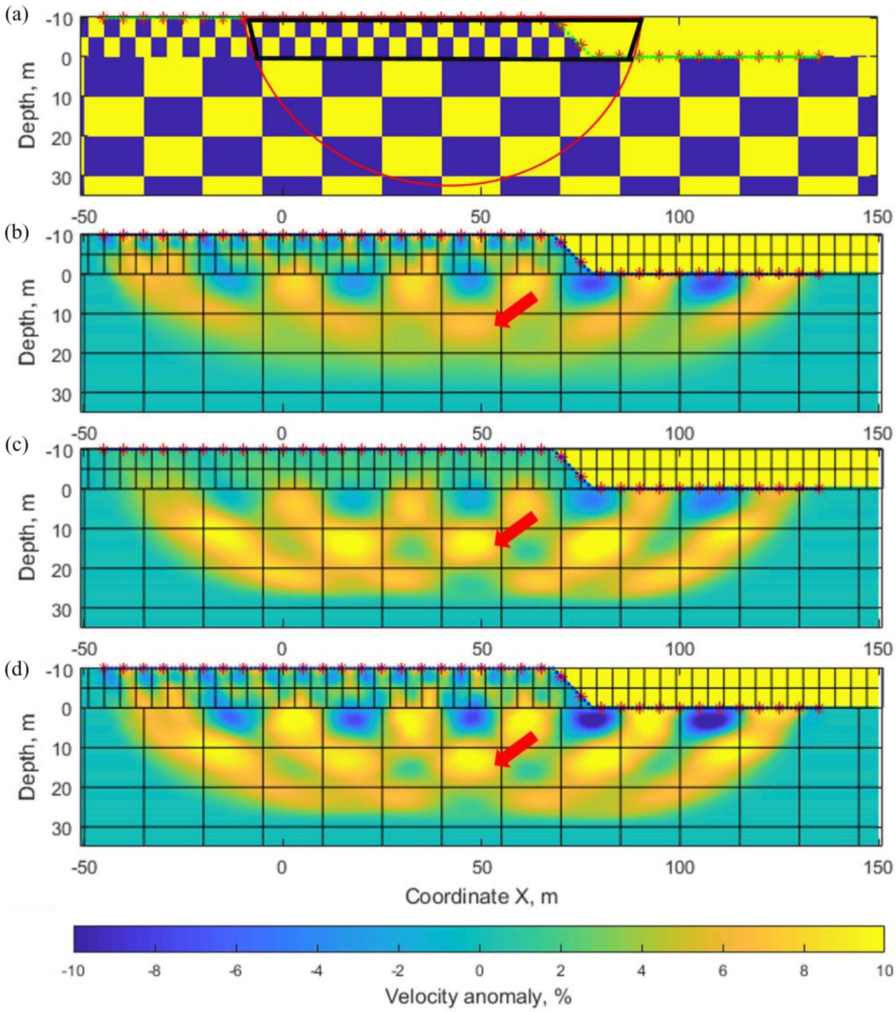

Figure 1 Checkboard test for comparing tomographic inversions after the first iteration: (a) true velocity anomalies (here red and black frames indicate regions used for quantitative error estimations for shallow and all depths correspondingly; see Table 1), (b) recovered anomalies for velocity parameterization, (c) same for slowness parameterization and (d) same for our new parameterization.

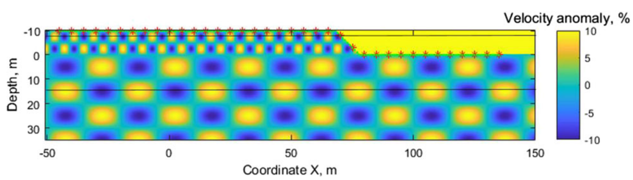

Figure 2 True velocity model with smooth anomalies; two depth levels for comparing tomographic inversion results are shown by black lines (see Fig. 3).

Note that the slowness and the velocity parameterizations mentioned above appear to be two particular cases of the general equation (6). We compare three variants of the model parameterization using the scaling rule described in equation (6):

- slowness parameterization, where $\sigma = 0$ or $w_{ii} = 1$;
- velocity parameterization, where $\sigma = 2$ or $w_{ii} = 1/v_{0i}^2$;
- new (intermediate) parameterization, where $\sigma = 1$ or $w_{ii} = 1/v_{0i}$.

SYNTHETIC TESTING OF DIFFERENT PARAMETERIZATIONS

Tomographic inversion is a non-linear problem. This non-linearity is addressed by iteratively solving the linear problem, shown in equation (4), and tracing rays in the updated velocity model after each iteration (Rawlinson and Sambridge, 2003). We apply the linear scaling of the model-parameter space (equation (5)) at each iteration (using the last updated

18730604, 2022, 2, Downloaded from https://onlinelibrary.wiley.com/doi/10.1002/nsg.12196 by Trofimuk Institute of Petroleum Geology and Geophysics SB RAS, Wiley Online Library on [28/11/2024]. See the Terms and Conditions (https://onlinelibrary.wiley.com/terms-and-conditions) on Wiley Online Library for rules of use; OA articles are governed by the applicable Creative Commons License

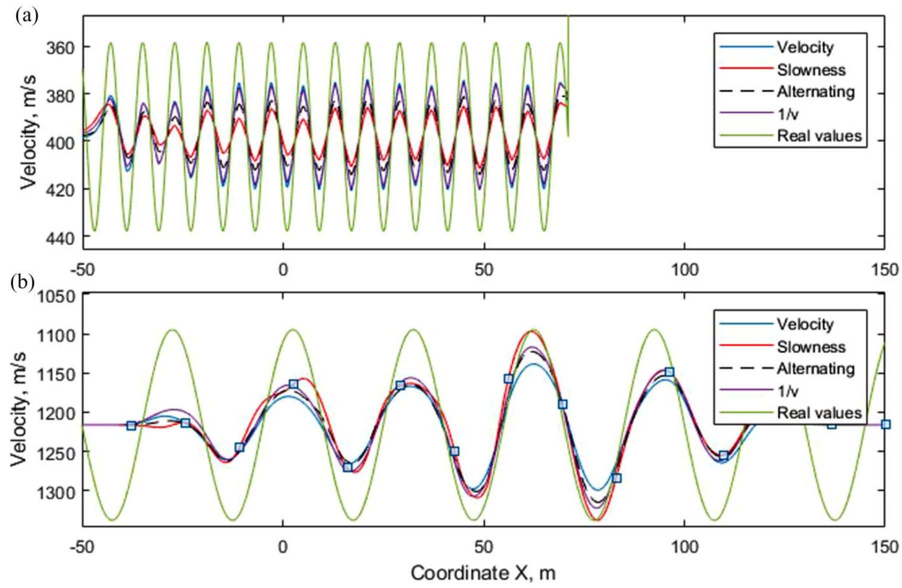

Figure 3 Comparison of tomographic inversion results at two depth levels (Fig. 2): 7.5 m (a) and 15.0 m (b); the green line shows true velocity variations and inversion results for different model parameterizations are shown by other colours (see legend).

velocity model as v_0), which results in a non-linear procedure. Thus, it is difficult to predict the influence of switching between model parameterizations on the final tomographic result. We further show a series of synthetic tests to study this problem.

For the tomographic inversion, we follow the strategy described by Koulakov *et al.* (2010). Specifically, we utilize the same linear system solvers and regularization method. For computing traveltimes and rays, we used the numerical eikonal solver from Nikitin *et al.* (2018), which implements the fast-sweeping algorithm (Zhao, 2005). To solve the system of linear equations, the Least Squares with QR-factorization (LSQR) method was used (Paige, 1982). We used the same initial model and 10 iterations of linear tomographic inversions for all tests. However, the result of the inversion also strongly depended on the smoothing and damping parameters (see, Koulakov *et al.*, 2010). Optimal smoothing and damping parameters were chosen separately for each model parameterization using the following criteria: minimal traveltime and velocity residuals, and visual assessment of the solution stability (no local high-amplitude anomalies in the recovered model perturbations).

Let us briefly mention the initial model-building strategy that is crucial for tomographic inversion. First, we invert traveltimes to build the initial model with a linear velocity growth with depth. Then we perform one iteration of tomographic inversion, compute the average of velocity anomalies at each depth and subtract them from the initial model. Note that the ray tomography updates the velocity model only in the region with good coverage of initially traced rays. For a given source–receiver offset, the maximum depth of the refracted ray penetration increases with the increasing gradient of the velocity growth. Therefore, it is better to take a slightly higher velocity gradient for the initial model as it results in deeper diving rays, that is better ray coverage with depth.

For the first synthetic test, we took the velocity model with superimposed velocity anomalies of the checkboard shape (Leveque et al., 1993) (see Fig. 1a), and anomaly amplitudes were ±10% of the reference linear gradient of increasing velocity. A linear gradient was expressed by the formula: $300 + 40 \times (z - z_0)$ m/s. Anomalies varied in size: 2.0×2.5 m for the shallow part, 15×10 m for the deeper part. Acquisition geometry and topography were typical for engineering seismology: source spacing was 5 m, receiver spacing was 1.0 m and profile length was 175 m. Receivers and sources are shown as green dots and red stars, respectively, in Figure 1.

The tomographic rectangular grid size was 1.0×2.0 m, and the initial velocity model was built as described earlier. We performed tomographic inversion for two classic model parameterizations: velocity parameterization (Fig. 1b) and slowness parameterization (Fig. 1c). One can see that the velocity parameterization ($\sigma = 2$) provides better results for the shallow part (small rectangles are better recovered), but the

18730604, 2022, 2, Downloaded from https://onlinelibrary.wiley.com/doi/10.1002/nsg.12196 by Trofimuk Institute of Petroleum Geology and Geophysics SB RAS, Wiley Online Library on [28/11/2024]. See the Terms and Conditions (https://onlinelibrary.wiley.com/terms-and-conditions) on Wiley Online Library for rules of use; OA articles are governed by the applicable Creative Commons License

18730604, 2022, 2, Downloaded from https://onlinelibrary.wiley.com/doi/10.1002/nsg.12196 by Trofimuk Institute of Petroleum Geology and Geophysics SB RAS, Wiley Online Library on [28/11/2024]. See the Terms and Conditions (https://onlinelibrary.wiley.com/terms-and-conditions) on Wiley Online Library for rules of use; OA articles are governed by the applicable Creative Commons License

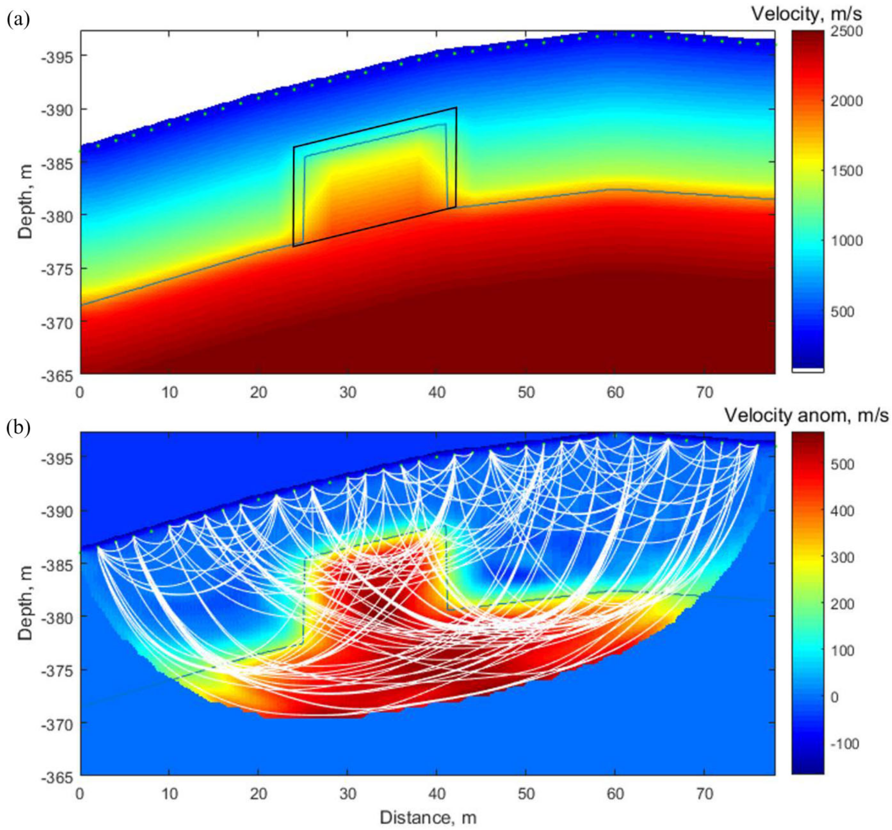

Figure 4 Test model with an uplifted block: (a) true velocity model, the black frame indicates the region of interest for quantitative estimation of the velocity misfit (Fig. 5); (b) velocity anomalies after ten iterations of tomographic inversion with the new parameterization, white lines – rays.

inversion quality degrades in the deeper part. The slowness parameterization ($\sigma = 0$) provides better results for the deeper part, but the inversion quality degrades in the shallow part. So it looks natural to try intermediate value ($\sigma = 1$) that we will further call a new parameterization ($1/v_{0i}$). The corresponding tomographic result is shown in Figure 1(d). One can clearly see that our new parameterization shows a good resolution for both – shallow and deeper parts (red arrows show deeper velocity anomaly for comparison).

For the quantitative comparison of the tomographic inversion results, we computed the mean absolute error between the true and the recovered velocity models for two regions: for the shallow part (thick black contour in Fig. 1a), and for all deeper parts (thin red contour in Fig. 1a). Corresponding errors for the three parameterizations are shown in Table 1. Note that the resultant time misfit was less than 1.0 ms for all parameterizations. These quantitative estimates confirm that our new parameterizations give the optimal result everywhere. Its mean-absolute error is very close to the velocity parameterization in the shallow part and very close to the slowness parameterization for the deeper part.

In addition, we tried another straightforward approach – to switch between the velocity and the slowness parameterizations after each tomographic iteration (so that tomography should switch its focus between the upper and lower parts of the model). This will be referred to as an alternating parameterization. Table 1 shows that such an alternating strategy does not perform better than our new parameterization.

Thus the velocity parameterization can be used if it is known that the velocity anomalies are present only in the shallow part of the model. The slowness parameterization can be used given that the velocity anomalies are present in the deeper part. Our new parameterization (New) gives optimal results for anomalies at all depths.

For the second test, we used a checkerboard model with smooth anomalies (Fig. 2). Acquisition geometry, background linear velocity gradient and the size of anomalies are the same as in the previous test. We compare tomographic

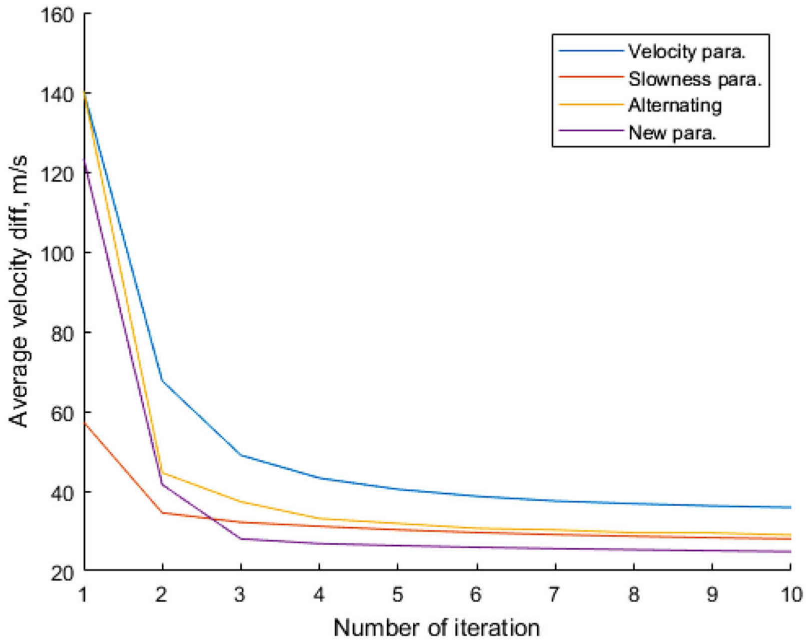

Figure 5 Mean absolute error between the true velocity model and tomographic inversion results in the region of interest (Fig. 4a) for a different number of iteration (horizontal axis) and different model parameterizations (line colour).

inversion results in Figure 3 at two depth levels, as shown by black lines in Figure 2 at depths of 7.5 m and 15.0 m. The green line shows real velocity values, recovered velocities for the velocity parameterization (blue line), the slowness parameterization (red line), alternating between the velocity and the slowness (orange line) and new parameterization (purple line). The velocity and the new (New) parameterizations perform the best at shallow depth (Fig. 3a); the slowness and the new (New) parameterizations are the best for the lower part (Fig. 3b). For this model, we also calculated the mean absolute error of the velocity reconstruction for all parameterizations. They are smaller in magnitude due to the smoothness of the model. However, comparative values are the same as in Table 1 so we do not show them here.

For the next synthetic test, we took a model with a ramp-shape anomaly (Fig. 4a). Acquisition system: the length of the seismic line was 78 m, the number of receivers was 40 (2.0 m apart) and the number of sources was nine (4 m apart). The tomographic grid size was 1.0 × 1.0 m, and the number of tomographic iterations was 10. Optimal smoothing and damping parameters were chosen as described earlier.

We performed tomographic inversions for all parameterizations resulting in the final time residuals less than 0.1 ms. For the quantitative comparison of parameterizations, we computed the mean absolute error between the inverted and the true velocity model in the vicinity of the anomaly (black parallelogram contour in Fig, 4a). Figure 5 shows the mean absolute errors for different parameterizations (line colour) at different tomographic iterations.

One can see that the new parameterization (New) shows the minimum error. Recovered velocity anomalies for parameterization are shown in Figure 4(b). Recovered values of the anomaly are about 30% higher than that for the velocity parameterization. This test again emphasizes the importance of choosing optimal parameterization for improving the quality of the tomographic inversion.

In addition, synthetic tests included sharp boundaries between layers, local velocity anomalies oriented vertically and horizontally (Fig. 6). Acquisition system: the length of the profile was 78 m, the number of receivers was 40 (2.0 m apart) and the number of sources was nine (8 m apart). The tomographic grid size was 1.0 × 1.0 m, and the number of tomographic iterations was 10. After tomographic inversion with different parameterizations, we evaluated the inversion quality by computing the mean absolute error between the true velocity model and the inversion result in the region surrounding the anomaly area; the order of values is the same as in Table 1. Misfits for the model with a sharp boundary (Fig. 6a) were 121, 120, 115 and 125. For the model with a vertical anomaly (Fig. 6b), misfits were 247, 309, 230, 247. For the model with a horizontal anomaly (Fig. 6c), misfits were 260, 260, 230, 230. The results confirm our overall conclusion that the new parameterization (New) provides optimal results – minimal or

18730604, 2022, 2, Downloaded from https://onlinelibrary.wiley.com/doi/10.1002/nsg.12196 by Trofimuk Institute of Petroleum Geology and Geophysics SB RAS, Wiley Online Library on [28/11/2024]. See the Terms and Conditions (https://onlinelibrary.wiley.com/terms-and-conditions) on Wiley Online Library for rules of use; OA articles are governed by the applicable Creative Commons License

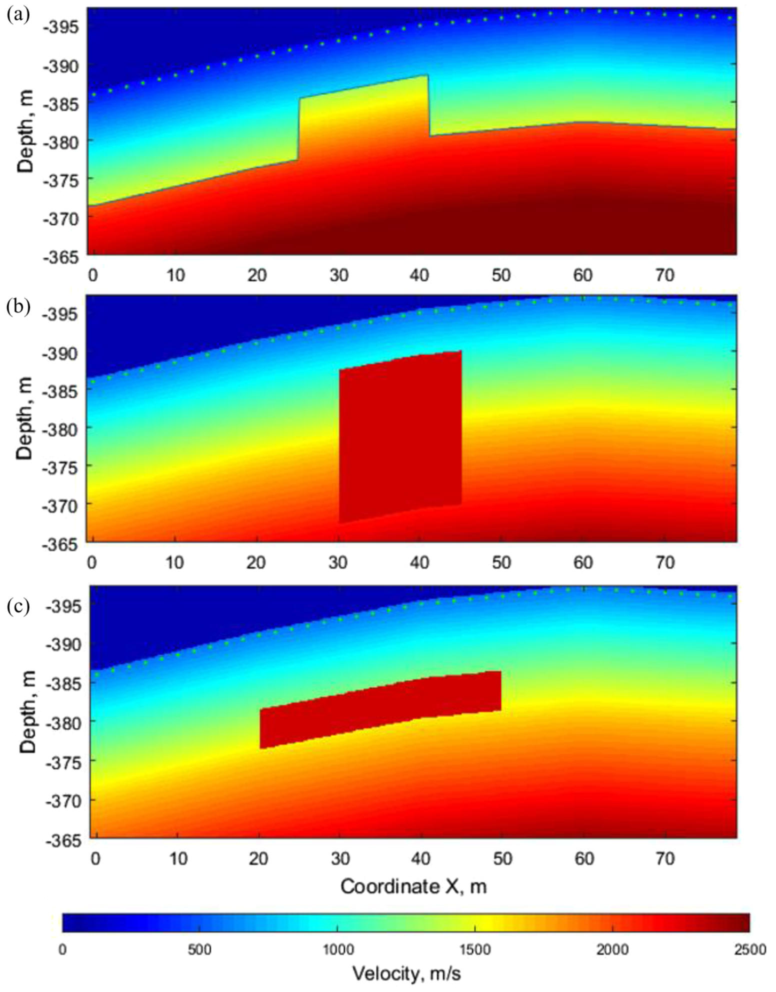

Figure 6 Velocity models used for synthetic tests: (a) sharp boundaries between layers, (b) vertically oriented anomaly and (c) horizontally oriented anomaly.

close to minimal errors for all testing models. Additional tests can be found in the Supporting Information.

REAL DATA EXAMPLE

Additionally, a real dataset from an engineering-seismology survey conducted in the area of perspective tunnel construction was used as a test. The area was characterized by considerable topography variations. Analysis of geological map indicated that a geological section should consist of three types of rocks: dispersed soils/clays; weathered gabbro–diorites; and gabbro–diorites.

The survey consisted of three-receiver layouts with a total number of 163 vertical and horizontal (perpendicular to the profile) receivers. The total profile length was 800 m. P-wave acquisition consisted of 25 sources, and gunpowder charges ignited in half-meter deep holes filled with water. S-wave acquisition consisted of 21 sledgehammer sources hits against walls of holes in the ground (25 × 40 cm). Each source included two hits in opposite directions perpendicular to the seismic profile. Records from these opposite hits were subtracted to suppress P-waves and strengthen S-waves. Observed first-break traveltimes for P- and S-waves are shown by black lines in Figure 7(a,b). Some shot gathers can be found in the Supporting Information.

We performed tomographic inversion of P- and S-wave traveltimes for all model parameterizations discussed earlier. The tomographic grid size was 2.0 × 7.0 m, and the number of tomographic iterations was 12. The smoothing and damping parameters for different parameterizations were selected as discussed above. Red lines in Figure 7(a,b) show the first-break traveltimes for P- and S-waves computed for the final tomographic models obtained in the new parameterization.

18730604, 2022, 2, Downloaded from https://onlinelibrary.wiley.com/doi/10.1002/nsg.12196 by Trofimuk Institute of Petroleum Geology and Geophysics SB RAS, Wiley Online Library on [28/11/2024]. See the Terms and Conditions (https://onlinelibrary.wiley.com/terms-and-conditions) on Wiley Online Library for rules of use; OA articles are governed by the applicable Creative Commons License

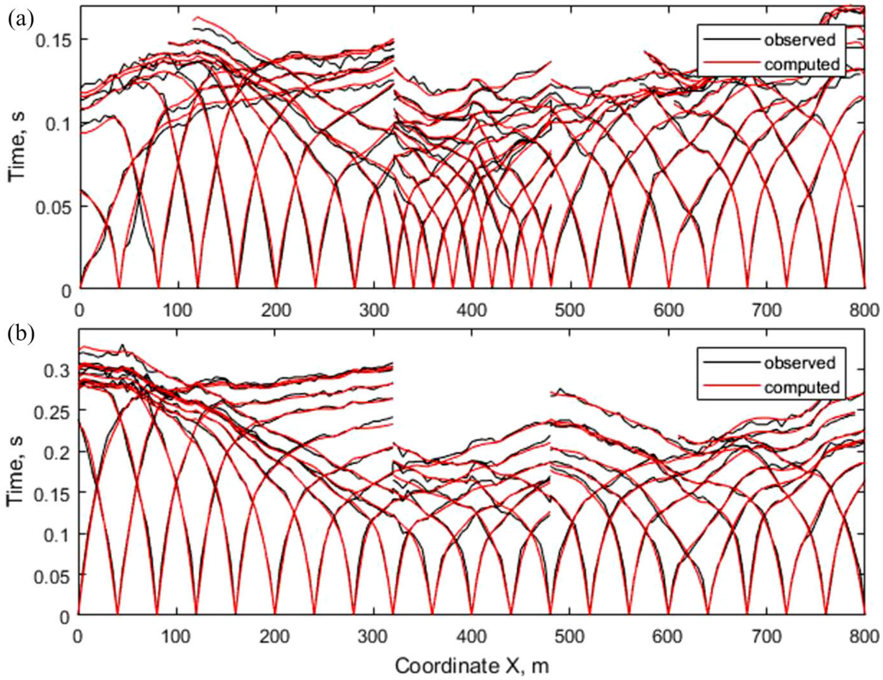

Figure 7 First-break traveltimes for (a) P-wave and (b) S-wave. Black lines are observed traveltimes from the survey, and red lines are traveltime from the result of tomographic inversion.

Resultant P-wave velocity models are shown in Figure 8, and the V_s/V_p ratio distributions are shown in Figure 9. In Figures 8 and 9, panels correspond to different parameterizations used during the tomographic inversion: (a) the velocity parameterization; (b) the slowness parameterization; (c) the alternating (velocity/slowness) parameterization; and (d) the new parameterization. In both figures, two black horizontal lines indicate planned tunnel location.

Although there are no sharp boundaries in smooth tomographic models, we introduce boundaries for interpretation by tracking iso-velocity lines (Zelt *et al*., 2003). Dashed lines in Figures 8 and 9 show P-wave velocity isolines corresponding to 2000 m/s and 3500 m/s. They separate three layers that we interpret as soils/clays, weathered gabbro–diorites, and gabbro–diorites (from top to bottom) based on *a priori* information. According to Goryainov (1992), water saturation lowers the V_s/V_p ratio, for dispersed soils it may get as low as 0.07. For cemented rocks, the value decreases down to 0.4–0.6. Thus, we interpret low V_s/V_p ratio anomalies as highly dispersed or water-saturated rocks. The maximum physically reasonable V_s/V_p ratio is 0.7 (higher values correspond to negative Poisson's ratio).

We used the final tomographic models to compute first-break traveltimes for P- and S-waves. Mean traveltime misfits for tomography with different parameterizations are the following (P-wave/S-wave): 2.29/3.50 ms for the velocity parameterization, 4.25/6.50 ms for the slowness parameterization, 3.21/3.50 ms for the alternating (velocity/slowness) parameterization, 1.81/3.00 ms was obtained for the New parameterization. The best traveltime misfit is reached when we use our new parameterization.

Let us compare the resultant models in Figures 8 and 9 in more detail. The velocity parameterization result (Fig. 8a) shows some details at shallow depth. However, the V_s/V_p model (Fig. 9a) contains many small anomalies with values exceeding 0.7, which is not physically reasonable. Thus we conclude that these anomalies appear from artefacts produced by the independent inversions for P- and S-waves. Then these artefacts are emphasized when inspecting the V_s/V_p ratio values. The slowness parameterization (Figs. 8b and 9b) results in large traveltime misfits exceeding all other parameterizations. This model is very smooth lacking clear anomalies that would help with the interpretation. The alternating parameterization result (Figs. 8c and 9c) provides a non-geologic anomaly on the left (see the green circle). Here we see the anomaly with a low V_s/V_p ratio that we associate with water-saturated disperse rocks. It is present in all of the tomographic results, but in Figure 9(c) this anomaly has very low values and spreads uphill, which does not look natural. There is also a large anomaly with a non-physically high V_s/V_p ratio

18730604, 2022, 2, Downloaded from https://onlinelibrary.wiley.com/doi/10.1002/nsg.12196 by Trofimuk Institute of Petroleum Geology and Geophysics SB RAS, Wiley Online Library on [28/11/2024]. See the Terms and Conditions (https://onlinelibrary.wiley.com/terms-and-conditions) on Wiley Online Library for rules of use; OA articles are governed by the applicable Creative Commons License

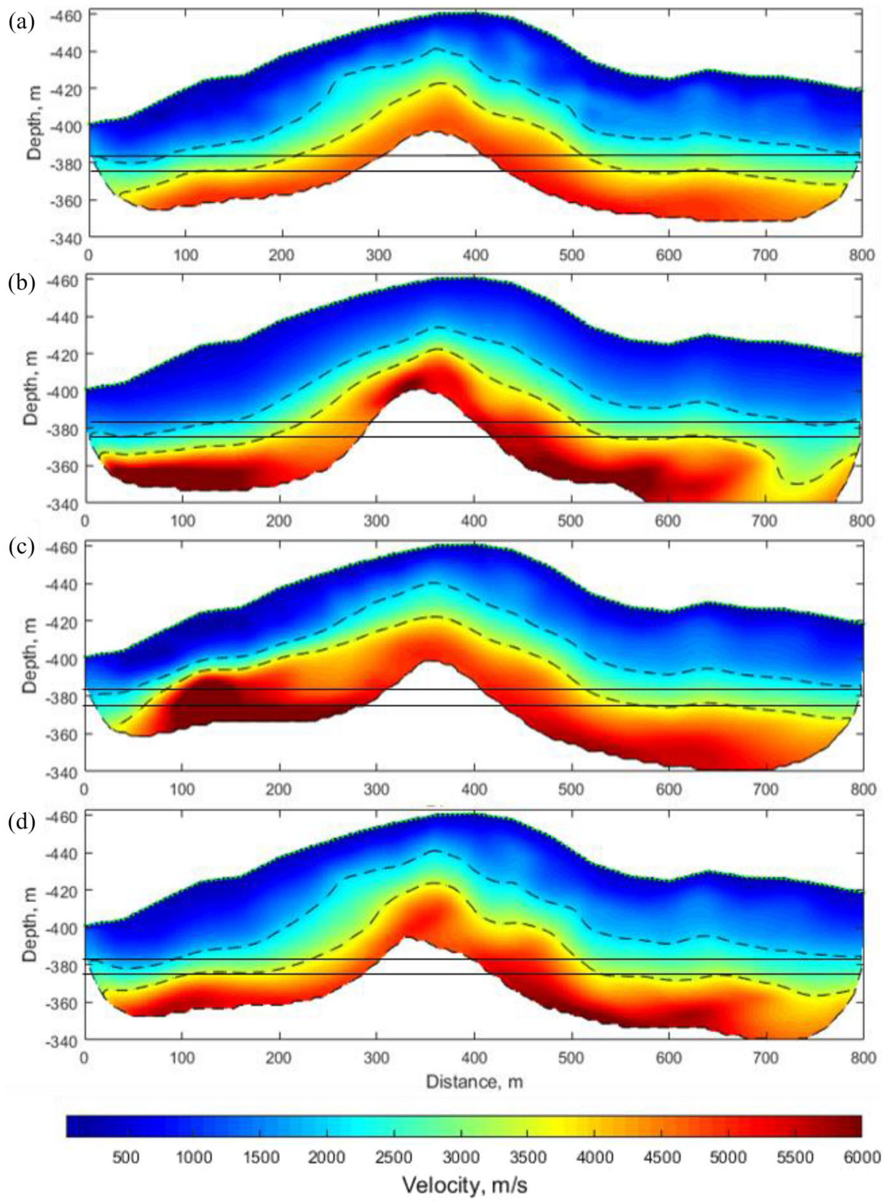

Figure 8 P-wave velocity (V_p) model from tomographic inversion for different model parameterizations: (a) velocity, (b) slowness, (c) alternating and (d) new parameterization; black solid lines are the planned tunnel location, and dashed lines are velocity isolines for 2000 and 3500 m/s.

exceeding 0.7 in the upper part. Our new parameterization (Figs. 8d and 9d) provides minimal traveltime misfits and does not contradict geological assumptions.

In our interpretation of the results, we focus on two anomalies with a low V_s/V_p ratio highlighted by green ellipses in Figure 9. Left anomaly (green circle): we interpret as a region of loosened water-saturated rocks that even spreads into the lower gabbro–diorite layer. The second anomaly (green ellipse): we interpret as a water-saturated fractured or fault zone. This interpretation is well supported by our new parameterization result (Fig. 9d); the anomaly with a low V_s/V_p ratio is clearly connected to the surface that is consistent with the interpretation of the water-saturated fractured zone. The overall conclusion is that the seismic survey revealed two zones of loosened water-saturated zones in the gabbro–diorite layer. Thus, the site is not recommended for tunnel construction unless additional drilling and geological studies are carried out.

18730604, 2022, 2, Downloaded from https://onlinelibrary.wiley.com/doi/10.1002/nsg.12196 by Trofimuk Institute of Petroleum Geology and Geophysics SB RAS, Wiley Online Library on [28/11/2024]. See the Terms and Conditions (https://onlinelibrary.wiley.com/terms-and-conditions) on Wiley Online Library for rules of use; OA articles are governed by the applicable Creative Commons License

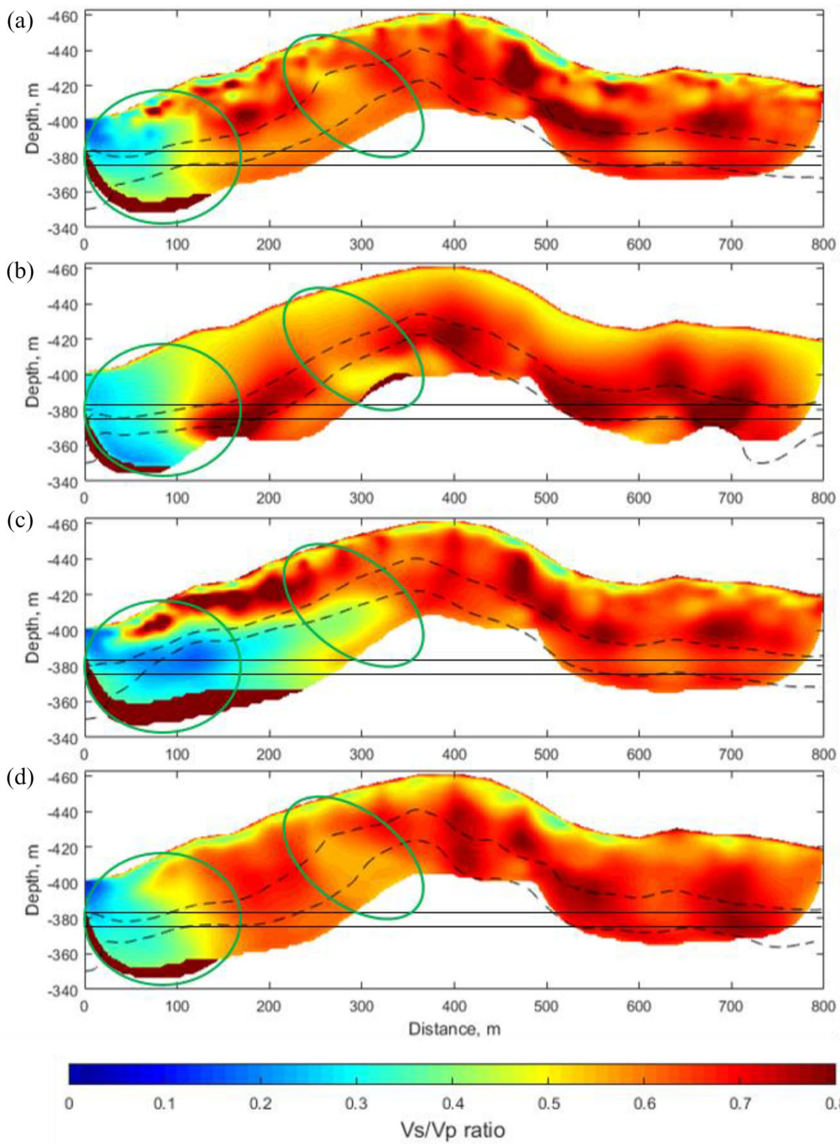

Figure 9 V_s/V_p ratio from tomographic results for different model parameterizations: (a) velocity, (b) slowness, (c) alternating, and (d) new parameterization; black solid lines are planned tunnel location, dashed lines are velocity isolines for 2000 and 3500 m/s, and green ellipses are areas of low V_s/V_p anomalies.

CONCLUSIONS

In this paper, we compared the results of tomographic inversion for different model parameterizations. For this comparison, we used the synthetics velocity model as well as a real engineering seismic data example. Our tests confirm that using a different weighting of the model parameterization changes the sensitivity of the tomographic inversion to anomalies at different depths.

Therefore, one can choose proper parameterization given the expected depth of velocity anomalies. When only shallow anomalies are expected, one can use the velocity parameterization. When only deep anomalies are expected, one can choose the slowness parameterization. In the general case, the new parameterization provides optimal results with good resolution of the recovered velocity anomalies at all depths within the region with good ray coverage.

Note that using the proposed parameterization does not require the development of a new algorithm of tomographic inversion. It requires modification of the tomographic matrix by applying a proper weighting matrix. Then one can proceed with any standard tomographic inversion algorithm.

18730604, 2022, 2, Downloaded from https://onlinelibrary.wiley.com/doi/10.1002/nsg.12196 by Trofimuk Institute of Petroleum Geology and Geophysics SB RAS, Wiley Online Library on [28/11/2024]. See the Terms and Conditions (https://onlinelibrary.wiley.com/terms-and-conditions) on Wiley Online Library for rules of use; OA articles are governed by the applicable Creative Commons License

ACKNOWLEDGEMENT

G. Chernyshov was supported by RFBR, project number 19-35-90114.

CONFLICT OF INTEREST

There is no conflict of interest.

DATA AVAILABILITY STATEMENT

The data that support the findings of this study are available on request from the corresponding author. The data are not publicly available due to privacy or ethical restrictions.

REFERENCES

Arciniega-Ceballos A., Hernandez-Quintero E., Cabral-Cano E., Morett-Alatorre L., Diaz-Molina O., Soler-Arechalde A. and Chavez-Segura R. (2009) Shallow geophysical survey at the archaeological site of San Miguel Tocuila, Basin of Mexico. *Journal of Archaeological Science*, 36(6), 1199–1205.

Cercato M. and De Donno G. (2018) Focusing on soil-foundation heterogeneity through high-resolution electrical and seismic tomography. *Near Surface Geophysics*, 16(1), 67–78.

Di Fiore V., Cavuoto G., Tarallo D., Punzo M. and Evangelista L. (2016) Multichannel analysis of surface waves and down-hole tests in the archeological "Palatine Hill" area (Rome, Italy): evaluation and influence of 2D effects on the shear wave velocity. *Surveys in Geophysics*, 37(3), 625–642.

Goryainov N.N. (1992) *Application of Seismoacoustic Methods in Hydrogeology and Engineering Geology*. Nedra, 261 p. (in Russian)

Hagedoorn J.G. (1959) The plus-minus method of interpreting seismic refraction sections. *Geophysical prospecting*, 7(2), 158–182. https://www.earthdoc.org/content/journals/10.1111/j.1365-2478.1964.tb01888.x.

Koulakov I., Stupina T. and Kopp H. (2010) Creating realistic models based on combined forward modeling and tomographic inversion of seismic profiling data. *Geophysics*, 75(3), B115–B136.

Lanz, E. and Maurer, H. and Green, A.G. (1998) Refraction tomography over a buried waste disposal site. *Geophysics*, 63(4), 1414–1433.

Leveque J.-J., Rivera L. and Wittlinger G. (1993) On the Use of the Checker-board test to assess the resolution of tomographic inversions. *Geophysical Journal International*, 115(1), 313–318. https://academic.oup.com/gji/article-abstract/115/1/313/604170.

Luo Y., Modrak R. and Tromp J. (2015) Strategies in adjoint tomography. *Handbook of Geomathematics*, 2nd edition. Springer, pp. 1943–2001.

Maries G., Ahokangas E., Makinen J., Pasanen A. and Malehmir A. (2016) Interlobate esker architecture and related hydrogeological features derived from a combination of high-resolution reflection seismic and refraction tomography, Virttaankangas, southwest Finland. *Hydrogeology Journal*, 25, 829–845.

Nikitin A.A., Serdyukov A.S. and Duchkov A.A. (2018) Cache-efficient parallel eikonal solver for multicore CPUs. *Computational Geosciences*, 22(3), 775–787.

Nolet G. (ed.) (2012) *Seismic Tomography: With Applications in Global Seismology and Exploration Geophysics*, Vol. 5. Springer Science & Business Media, 385 p.

Nolet G. (1987) Seismic wave propagation and seismic tomography. In *Seismic Tomography*. Springer, pp. 1–23.

Palmer D. (2015) Is accuracy more important than precision in near-surface refraction seismology?. *Near Surface Geophysics*, 13(1), 1–18.

Paige C. and Saunders M. (1982) LSQR: An algorithm for sparse linear equations and sparse linear least squares. *ACM Transactions on Mathematical Software*, 8(1), 43–71. https://dl.acm.org/doi/pdf/10.1145/355984.355989.

Park C.B., Miller R.D. and Xia J. (1999) Multichannel analysis of surface waves. *Geophysics*, 64(3), 800–808. https://library.seg.org/doi/abs/10.1190/1.1444590.

Rawlinson N. and Sambridge M. (2003) Seismic traveltime tomography of the crust and lithosphere. *Advances in Geophysics*, 46, 81–199.

Schicht T., Lindner U., Heckner J., Strobel G. and Rappsilber I. (2007) Seismic tomography on the castle hill in Quedlinburg. *Near Surface Geophysics*, 5(5), 339–343.

Sun R., Kaslilar A. and Juhlin C. (2020) Reprocessing of high-resolution seismic data for imaging of shallow groundwater resources in glacial deposits, SE Sweden. *Near Surface Geophysics*, 18(5), 545–559.

Suvorov V.D., Mishenkina Z.M., Petrick G.V., Sheludko I.F., Seleznev V.S. and Solovyov V.M. (2002) Structure of the crust in the Baikal rift zone and adjacent areas from deep seismic sounding data. *Tectonophysics*, 351(1-2), 61–74.

Tikhotskii S.A., Fokin I.V. and Schur D.Y. (2011) Traveltime seismic tomography with adaptive wavelet parameterization. *Izvestiya, Physics of the Solid Earth*, 47(4), 326–344.

Trabi B. (2018) *Comparison of Slowness vs. Velocity Perturbations in Bayesian Seismic Inversion*. Leoben: Leoben University, 75 p.

Tong P., Yang D. and Huang X. (2019) Multiple-grid model parametrization for seismic tomography with application to the San Jacinto fault zone. *Geophysical Journal International*, 218(1), 200–223.

Yilmaz Ö. (2015) *Engineering Seismology with Applications to Geotechnical Engineering*. SEG, 964 p.

Varga L., Balázs P. and Nagy A. (2015) Discrete tomographic reconstruction via adaptive weighting of gradient descents. *Computer Methods in Biomechanics and Biomedical Engineering: Imaging & Visualization*, 3(2), 101–109.

Zelt C.A. (2011) Traveltime tomography using controlled-source seismic data. *Encyclopedia of Solid Earth Geophysics*, 1453–1473.

Zelt C.A. and Smith R.B. (1992) Seismic traveltime inversion for 2-D crustal velocity structure. *Geophysical Journal International*, 108(1), 16–34.

Zelt C.A., Sain K., Naumenko J.V. and Sawyer D.S. (2003) Assessment of crustal velocity models using seismic refraction and reflection tomography. *Geophysical Journal International*, 153(3), 609–626.

18730604, 2022, 2, Downloaded from https://onlinelibrary.wiley.com/doi/10.1002/nsg.12196 by Trofimuk Institute of Petroleum Geology and Geophysics SB RAS, Wiley Online Library on [28/11/2024]. See the Terms and Conditions (https://onlinelibrary.wiley.com/terms-and-conditions) on Wiley Online Library for rules of use; OA articles are governed by the applicable Creative Commons License

Zhao H.A. (2005) Fast sweeping method for eikonal equations. *Mathematics of Computation*, 74(250), 603–627.

SUPPORTING INFORMATION

Additional supporting information may be found online in the Supporting Information section at the end of the article.

Figure 1 The initial and true model for the first synthetic test.

Figure 2 Results of check-board test with smooth anomaly's for the velocity parameterization (a), the slowness parameterization (b), alternating (velocity/slowness) parameterization (c), new parameterization 1/v (d)

Figure 3 initial velocity model for all of the following synthetic tests

Figure 4 Results of synthetic test with uplifted block for the velocity parameterization (a), the slowness parameterization (b), alternating (velocity/slowness) parameterization (c), new parameterization 1/v (d)

Figure 5 Results of synthetic test with sharp boundary for the velocity parameterization (a), the slowness parameterization (b), alternating (velocity/slowness) parameterization (c), new parameterization 1/v (d)

Figure 6 Results of synthetic test with vertical oriented anomaly for the velocity parameterization (a), the slowness parameterization (b), alternating (velocity/slowness) parameterization (c), new parameterization 1/v (d)

Figure 7 Results of synthetic test with horizontal oriented anomaly for the velocity parameterization (a), the slowness parameterization (b), alternating (velocity/slowness) parameterization (c), new parameterization 1/v (d)

Figure 8 S-wave shot gather: upper panel is the S-wave gather with first break picks (red line); lower row shows gathers from two opposite hits.

Figure 9 P-wave shot gather with first break picks (green line)

18730604, 2022, 2, Downloaded from https://onlinelibrary.wiley.com/doi/10.1002/nsg.12196 by Trofimuk Institute of Petroleum Geology and Geophysics SB RAS, Wiley Online Library on [28/11/2024]. See the Terms and Conditions (https://onlinelibrary.wiley.com/terms-and-conditions) on Wiley Online Library for rules of use; OA articles are governed by the applicable Creative Commons License